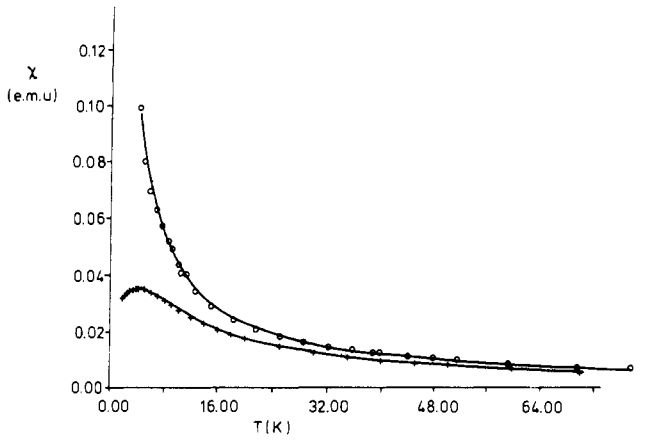

Figure 4. Magnetic susceptibility curves for **1** (+) and **2** (○), together with a theoretical curve corresponding to a Heisenberg chain (J = −2.54 cm^{-1} (**1**); J = −0.25 cm^{-1} (**2**)).

compared with the silver compound, in which this absorption is observed at 1670 cm^{-1}, it may be concluded that the silver–oxygen coordination has a much smaller effect than the hydrogen bridging in our compounds, in accordance with the semicoordination found (Ag–O = 2.78 Å). The ligand field spectra (Table V) of **1** and **2** both agree with a distorted octahedral coordination. The difference in the positions of the maxima results from the difference in chromophores and the degree of distortion. Table V also lists the ESR g values. The rhombic symmetry around the copper ions is reflected by the occurrence of three g values. The larger difference for g_2 and g_3 in compound **2** is attributed to the much larger rhombic distortion of **2** compared to that of **1**.

Magnetic Susceptibilities. Figure 4 shows the magnetic susceptibility measurements as a function of the temperature. From the structure analyses it was not quite clear which dimensionality in the magnetic interactions was applicable, because no unambiguous assignment of exchange paths was possible. Preliminary investigations, however, suggested that a one-dimensional copper–copper interaction was sufficient to account for the observed data, which have thus been fitted to such a model[25] (the calculated curves are also drawn in the fugure). The resulting difference in the antiferromagnetic interaction can then be attributed to a difference in electron distribution in the ground state. The two compounds have a different tetragonal distortion, because of which a greater unpaired electron density in the equatorial $d_{x^2-y^2}$ orbital is expected for **1**. In the case of **2** a larger part of the unpaired electron density will be in d_{z^2}, because here we have a weaker (equatorial) ligand field. This d_{z^2} orbital can have no interaction with the ligand π system, because it is in the same plane as the rings, as is seen from inspection of Figures 2 and 3. This implies at the same time that the copper–copper interaction must be transmitted through the stacking of the ligands and not through hydrogen bridges: in **1** there are no hydrogen bridges between the equatorial planes of adjacent copper ions (see Table IV). Further investigations on this matter in connection with the dimensionality of the interaction are in progress.

Concluding Remarks

The present structures show that triazolopyrimidines offer interesting material for mimicking nucleic bases in metal compounds. This study also shows that these types of ligands have stacking possibilities that not only determine the packing in the crystal but may also play an interesting role in the magnetic interactions that metal ions in bioinorganic model compounds can have.

Acknowledgment. We are indebted to Dr. R. A. G. de Graaff for his advice on solving the structures, to Dr. W. Vreugdenhil for his assistance in measuring the magnetic susceptibilities, and to the Leiden Materials Science Centre (Werkgroep Fundamenteel Materialenonderzoek) for support.

Supplementary Material Available: Tables SIII and SIV, listing the positional parameters and isotropic temperature factors of the hydrogen atoms, and Tables SV and SVI, listing anisotropic parameters of the non-hydrogen atoms (2 pages); Tables SI and SII, listing calculated and observed structure factors (11 pages). Ordering information is given on any current masthead page.

(25) Estes, W. E.; Hatfield, W. E.; van Ooijen, J. A. C.; Reedijk, J. *J. Chem. Soc., Dalton Trans.* **1980**, 2121.

Contribution from the Department of Chemistry, University of California, Davis, California 95616

Low-Coordinate Lead(II) Complexes with PbP_2C and PbP_4 Coordination. Preparations and Structures of $Pb[(Ph_2P)_2CH]_2$ and $Pb[(Ph_2P)_2C(SiMe_3)]_2$

Alan L. Balch* and Douglas E. Oram

Received November 13, 1986

The reaction between $PbCl_2$ and $LiCH(PPh_2)_2$ in tetrahydrofuran yields, after cooling and addition of ethyl ether, orange crystals of $Pb[(Ph_2P)_2CH]_2\cdot(CH_3CH_2)_2O$. They crystallize in the monoclinic space group $P2_1/c$ (No. 14) with a = 18.075 (8) Å, b = 14.713 (6) Å, c = 18.099 (8) Å, β = 92.29 (4)°, V = 4810 (4) Å^3, and Z = 4 at 130 K. Refinement yielded R = 0.0571 for 3899 reflections with $I > 3\sigma(I)$ and 272 parameters. The lead is pyramidal with bonds to two phosphorus atoms of a chelating $(Ph_2P)_2CH^-$ and to one carbon of a monodentate $(Ph_2P)_2CH^-$. A similar reaction between $PbCl_2$ and $Li(Ph_2P)_2C(SiMe_3)$ yields $Pb[(Ph_2P)_2C(SiMe_3)]_2$. This crystallizes from ethyl ether as orange crystals that belong to the orthorhombic space group $P2_12_12_1$ (No. 19) with a = 17.25 (4) Å, b = 11.331 (12) Å, c = 26.60 (4) Å, V = 5200 (10) Å^3, and Z = 4 at 130 K. Refinement yielded R = 0.053 for 2783 reflections with $I > 3\sigma(I)$ and 288 parameters. The structure contains lead bound to the four phosphorus atoms of the two chelating ligands in a distorted-trigonal-bipyramidal geometry with a stereochemically active lone pair. The ^{31}P NMR spectra of both complexes indicate fluxionality. In $Pb[(Ph_2P)_2CH]_2$ the two inequivalent ligands become equivalent in solution at 70 °C, while in $Pb[(Ph_2P)_2C(SiMe_3)]_2$ the two distinct types of phosphorus atoms become equivalent.

Introduction

The structures of lead(II) complexes and the role of the potential lone pair in determining their geometries are poorly defined at present.[1] A wide variation in stoichiometry of lead(II) complexes has been noted.[2] The structures of many species that have been characterized show high coordination numbers, which are frequently achieved through polymerization.[3]

(1) Greenwood, N. N.; Earnshaw, A. *Chemistry of the Elements*; Pergamon: Oxford, England, 1984; p 445.

(2) Abel, E. W. *Comprehensive Inorganic Chemistry*; Pergamon: Oxford, England, 1973; Vol. 2, pp 105–146.

(3) For examples, see: (a) Dean, P. A. W.; Vittal, J. J.; Payne, N. C. *Inorg. Chem.* **1985**, *24*, 3594. (b) Harrison, P. G.; Steel, A. T. *J. Organomet. Chem.* **1982**, *239*, 105. (c) Lawton, S. L.; Kokotailo, G. T. *Inorg. Chem.* **1972**, *11*, 363.

0020-1669/87/1326-1906$01.50/0

Table I. Atom Coordinates ($\times 10^4$) and Temperature Factors ($Å^2 \times 10^3$) for $Pb[(Ph_2P)_2CH]_2$ (**1**)

atom	x	y	z	U	atom	x	y	z	U
Pb	3076 (1)	6513 (1)	5735 (1)	21 (1)[a]	C(25)	4313 (7)	7385 (9)	7023 (7)	28 (4)
P(1)	3161 (2)	8547 (3)	6634 (2)	26 (1)[a]	C(26)	2796 (7)	6416 (10)	3876 (7)	27 (3)
P(2)	1690 (2)	8135 (3)	5702 (2)	27 (1)[a]	C(27)	2150 (7)	4766 (9)	4515 (7)	25 (4)
P(3)	2196 (2)	6012 (2)	4506 (2)	23 (1)[a]	C(28)	2283 (8)	4273 (10)	3897 (9)	43 (4)
P(4)	3588 (2)	6856 (2)	4347 (2)	21 (1)[a]	C(29)	2269 (8)	3319 (11)	3900 (9)	52 (5)
O	1653 (6)	3864 (7)	8132 (5)	50 (3)	C(30)	2154 (8)	2852 (11)	4563 (8)	46 (5)
C(1)	2669 (7)	8043 (8)	5786 (7)	19 (3)	C(31)	2026 (8)	3358 (11)	5197 (8)	50 (5)
C(2)	1347 (8)	7223 (9)	6285 (7)	30 (4)	C(32)	2046 (7)	4305 (9)	5192 (8)	32 (4)
C(3)	621 (8)	6920 (9)	6085 (8)	34 (4)	C(33)	1257 (7)	6333 (8)	4227 (6)	20 (3)
C(4)	317 (9)	6202 (10)	6479 (8)	44 (5)	C(34)	1146 (8)	7130 (10)	3820 (7)	37 (4)
C(5)	710 (8)	5812 (11)	7061 (8)	48 (5)	C(35)	431 (7)	7433 (10)	3623 (7)	35 (4)
C(6)	1414 (7)	6096 (9)	7265 (8)	31 (4)	C(36)	−168 (8)	6936 (10)	3838 (8)	42 (4)
C(7)	1723 (8)	6819 (9)	6895 (7)	35 (4)	C(37)	−58 (8)	6113 (9)	4197 (7)	34 (4)
C(8)	1449 (8)	9134 (10)	6241 (8)	32 (4)	C(38)	646 (7)	5837 (10)	4401 (7)	31 (4)
C(9)	1276 (7)	9139 (10)	7000 (8)	33 (4)	C(39)	4456 (7)	6306 (10)	4118 (8)	36 (4)
C(10)	1096 (8)	9926 (10)	7357 (9)	43 (4)	C(40)	5009 (8)	6183 (10)	4646 (9)	51 (5)
C(11)	1116 (8)	10753 (10)	6971 (8)	37 (4)	C(41)	5706 (10)	5815 (11)	4437 (9)	64 (6)
C(12)	1252 (9)	10772 (12)	6236 (9)	52 (5)	C(42)	5743 (11)	5556 (13)	3711 (11)	81 (7)
C(13)	1430 (8)	9977 (10)	5875 (8)	38 (4)	C(43)	5207 (11)	5633 (13)	3220 (11)	82 (7)
C(14)	3278 (7)	9745 (9)	6362 (7)	27 (4)	C(44)	4543 (9)	6028 (11)	3420 (9)	56 (5)
C(15)	3310 (7)	10063 (9)	5647 (8)	32 (4)	C(45)	3754 (6)	8022 (8)	4043 (6)	11 (3)
C(16)	3374 (8)	11000 (10)	5528 (9)	47 (5)	C(46)	4444 (7)	8383 (10)	3994 (6)	27 (3)
C(17)	3420 (7)	11595 (12)	6113 (7)	44 (4)	C(47)	4529 (8)	9296 (9)	3793 (7)	32 (4)
C(18)	3410 (8)	11312 (11)	6808 (9)	56 (5)	C(48)	3914 (7)	9833 (10)	3622 (7)	37 (4)
C(19)	3345 (8)	10382 (10)	6947 (8)	38 (4)	C(49)	3227 (8)	9468 (10)	3657 (7)	33 (4)
C(20)	4110 (7)	8096 (9)	6547 (7)	27 (4)	C(50)	3140 (7)	8562 (10)	3877 (6)	29 (3)
C(21)	4589 (7)	8361 (10)	6011 (7)	27 (3)	C(51)	2671 (8)	3745 (11)	7312 (10)	64 (6)
C(22)	5285 (8)	7943 (9)	5957 (8)	37 (4)	C(52)	1873 (7)	3519 (12)	7432 (7)	43 (4)
C(23)	5474 (9)	7264 (10)	6430 (8)	43 (4)	C(53)	916 (8)	3657 (11)	8280 (8)	60 (5)
C(24)	5011 (8)	6973 (11)	6976 (8)	48 (5)	C(54)	729 (10)	4126 (12)	8976 (8)	62 (6)

[a] Equivalent isotropic U defined as one-third of the trace of the orthogonalized U_{ij} tensor.

Here we report on the preparations and structures of two new neutral, homoleptic lead complexes. These contain Pb–P and Pb–C bonds and are among the first structurally characterized examples of lead(II) bonding to these elements. Although a number of lead(II) complexes with sulfur donors are well characterized,[3a,3c,4-8] few complexes of lead(II) with phosphorus donors have been reported[9-12] and only one is structurally characterized.[13] In this work we have examined the reaction of the ambidentate ligands [14,15] bis(diphenylphosphino)methanide $[(Ph_2P)_2CH^-]$ and its trimethylsilyl-substituted analogue $[(Ph_2P)_2C(SiMe_3)^-]$ with anhydrous lead(II) chloride. These ligands have the potential for binding through phosphorus or carbon and offer an unusual combination of donor abilities.

Preliminary descriptions of some of this work have appeared.[16,17]

Results

The reaction between anhydrous lead(II) chloride and $Li[CH(PPh_2)_2]$[18] in tetrahydrofuran yields a orange solution containing finely divided lead metal. Concentration, addition of ethyl ether, filtration, and cooling produces orange crystals of $Pb[(Ph_2P)_2CH]_2 \cdot (C_2H_5)_2O$ (**1**) in 55% yield. The analogous reaction between lead(II) chloride and $Li[(Ph_2P)_2C(SiMe_3)]$[19] yields a clear orange solution without precipitation of metallic lead. From this orange crystals of $Pb[(Ph_2P)_2C(SiMe_3)]_2$ (**2**) are obtained in 82% yield after filtration and cooling. Both complexes dissolve readily in tetrahydrofuran and toluene to give very air-sensitive orange solutions. They have moderate solubility in ethyl ether and do not dissolve in hexane. As solids both **1** and **2** darken during exposure to air for an hour.

Table II. Selected Interatomic Distances (Å) and Angles (deg) for $Pb[(Ph_2P)_2CH]_2$ (**1**)

Distances			
Pb–P(3)	2.782 (4)	Pb–P(4)	2.758 (4)
Pb–C(1)	2.371 (12)	P(1)–C(1)	1.895 (12)
P(1)–C(14)	1.845 (14)	P(1)–C(20)	1.851 (14)
P(2)–C(1)	1.775 (13)	P(2)–C(2)	1.830 (14)
P(2)–C(8)	1.826 (15)	P(3)–C(26)	1.713 (13)
P(3)–C(27)	1.835 (14)	P(3)–C(33)	1.814 (12)
P(4)–C(26)	1.759 (13)	P(4)–C(39)	1.828 (14)
P(4)–C(45)	1.830 (12)		
Angles			
P(3)–Pb–P(4)	61.5 (1)	P(3)–Pb–C(1)	96.6 (3)
P(4)–Pb–C(1)	88.7 (3)	C(1)–P(1)–C(14)	102.3 (6)
C(1)–P(1)–C(20)	101.4 (6)	C(14)–P(1)–C(20)	101.7 (6)
C(1)–P(2)–C(2)	104.7 (6)	C(1)–P(2)–C(8)	105.9 (6)
C(2)–P(2)–C(8)	100.9 (7)	Pb–P(3)–C(26)	94.7 (4)
Pb–P(3)–C(27)	106.4 (4)	C(26)–P(3)–C(27)	112.5 (7)
Pb–P(3)–C(33)	130.7 (4)	C(26)–P(3)–C(33)	109.6 (6)
C(27)–P(3)–C(33)	102.8 (6)	Pb–P(4)–C(26)	94.5 (4)
Pb–P(4)–C(39)	116.6 (5)	C(26)–P(4)–C(39)	114.6 (6)
Pb–P(4)–C(45)	120.7 (4)	C(26)–P(4)–C(45)	109.8 (6)
C(39)–P(4)–C(45)	101.3 (6)	Pb–C(1)–P(2)	112.3 (6)
Pb–C(1)–P(1)	105.5 (5)	P(3)–C(26)–P(4)	109.3 (7)
P(1)–C(1)–P(2)	118.2 (7)		

X-ray Crystal Structure of $Pb[(Ph_2P)_2CH]_2 \cdot (C_2H_5)_2O$ (1). Final atomic positional and thermal parameters are given in Table I. Table II contains selected interatomic distances and angles. One molecule of **1** crystallizes along with one molecule of ether in the

(4) Ito, T. *Acta Crystallogr., Sect. B: Struct. Crystallogr. Cryst. Chem.* **1972**, *B28*, 1034.
(5) Iwasaki, H.; Hagihara, H. *Acta Crystallogr., Sect. B: Struct. Crystallogr. Cryst. Chem.* **1972**, *B28*, 507.
(6) Dean, P. A. W.; Vittal, J. J.; Payne, N. C. *Inorg. Chem.* **1984**, *23*, 4232.
(7) Hagihara, H.; Yamashita, S. *Acta Crystallogr.* **1966**, *21*, 350.
(8) Hagihara, H.; Yoshida, N.; Watanabe, Y. *Acta Crystallogr., Sect. B: Struct. Crystallogr. Cryst. Chem.* **1969**, *B25*, 1775.
(9) duMont, W.-W.; Kroth, H.-J. *Angew. Chem., Int. Ed. Engl.* **1977**, *16*, 792.
(10) duMont, W.-W.; Neudert, B. *Z. Z. Anorg. Allg. Chem.* **1978**, *441*, 86.
(11) Dean, P. A. W.; Phillips, D. D.; Polensek, L. *Can. J. Chem.* **1981**, *59*, 50.
(12) Dean, P. A. W. *Can. J. Chem.* **1983**, *61*, 1795.
(13) Arif, A. M.; Cowley, A. H.; Jones, R. A.; Power, J. M. *J. Chem. Soc., Chem. Commun.* **1986**, 1446.
(14) Appel, R.; Haubrich, G.; Knoch, F. *Chem. Ber.* **1984**, *117*, 2063.
(15) Karsch, H. H. *Angew. Chem., Int. Ed. Engl.* **1982**, *21*, 921.
(16) Balch, A. L.; Oram, D. E. *Organometallics.* **1986**, *5*, 2159.
(17) Balch, A. L.; Oram, D. E. *Phosphorus Sulfur.*, in press.
(18) Brauer, D. J.; Hietkamp, S.; Stelzer, O. *J. Organomet. Chem.* **1986**, *299*, 137.
(19) Appel, R.; Geisler, K.; Scholer, H. F. *Chem. Ber.* **1979**, *112*, 648.

Table III. Atomic Coordinates ($\times 10^4$) and Isotropic Thermal Parameters ($Å^2 \times 10^3$) for $Pb[(Ph_2P)_2C(SiMe_3)]_2$ (**2**)

atom	x	y	z	U	atom	x	y	z	U
Pb	2244 (1)	6422 (1)	4243 (1)	28 (1)[a]	C(26)	2820 (13)	1681 (18)	2560 (7)	39 (5)
P(1)	2766 (4)	7323 (4)	3360 (2)	27 (2)[a]	C(27)	2166 (15)	2215 (21)	2386 (8)	48 (6)
P(2)	1970 (3)	5149 (5)	3283 (2)	29 (2)[a]	C(28)	1852 (14)	3210 (19)	2612 (8)	41 (6)
P(3)	3313 (3)	4912 (5)	4635 (2)	30 (2)[a]	C(29)	3765 (11)	5838 (18)	5033 (7)	24 (5)
P(4)	3436 (4)	7289 (5)	4911 (2)	35 (2)[a]	C(30)	4598 (12)	3848 (19)	5579 (7)	36 (6)
Si(1)	2407 (4)	6487 (6)	2248 (2)	39 (2)[a]	C(31)	4467 (12)	6350 (24)	6082 (8)	42 (5)
Si(2)	4597 (4)	5509 (6)	5458 (2)	36 (2)[a]	C(32)	5584 (16)	5950 (24)	5183 (10)	59 (8)
C(1)	2325 (11)	6362 (18)	2936 (6)	24 (4)	C(33)	2887 (13)	7938 (19)	5442 (7)	34 (6)
C(2)	3112 (14)	5388 (22)	1966 (8)	43 (6)	C(34)	2672 (15)	9113 (21)	5430 (8)	45 (6)
C(3)	1446 (15)	6208 (24)	1948 (9)	61 (8)	C(35)	2214 (15)	9563 (22)	5817 (9)	54 (6)
C(4)	2802 (16)	8033 (21)	2067 (8)	47 (6)	C(36)	1899 (15)	8826 (23)	6183 (9)	57 (7)
C(5)	3752 (12)	7719 (20)	3161 (8)	37 (6)	C(37)	2082 (13)	7619 (20)	6164 (8)	40 (6)
C(6)	4287 (13)	6775 (22)	3048 (8)	43 (6)	C(38)	2547 (11)	7209 (19)	5813 (8)	38 (6)
C(7)	5032 (15)	6993 (23)	2917 (9)	48 (6)	C(39)	4278 (12)	8324 (19)	4863 (7)	35 (6)
C(8)	5325 (17)	8141 (23)	2873 (10)	61 (8)	C(40)	4534 (12)	9023 (18)	5237 (8)	33 (5)
C(9)	4799 (16)	9076 (25)	2981 (9)	59 (8)	C(41)	5193 (14)	9624 (22)	5196 (9)	44 (6)
C(10)	4039 (13)	8860 (20)	3113 (8)	38 (6)	C(42)	5634 (14)	9590 (21)	4753 (8)	39 (6)
C(11)	2299 (12)	8753 (17)	3410 (6)	27 (4)	C(43)	5337 (14)	8931 (19)	4364 (8)	44 (6)
C(12)	2531 (12)	9500 (19)	3825 (8)	34 (6)	C(44)	4693 (13)	8238 (21)	4419 (8)	43 (6)
C(13)	2174 (16)	10596 (22)	3899 (8)	51 (6)	C(45)	4022 (12)	3915 (18)	4310 (8)	36 (5)
C(14)	1575 (16)	10851 (24)	3603 (9)	56 (7)	C(46)	4525 (13)	4518 (22)	4002 (8)	38 (6)
C(15)	1290 (13)	10135 (20)	3226 (8)	41 (6)	C(47)	5036 (14)	3799 (22)	3704 (9)	49 (7)
C(16)	1678 (13)	9064 (20)	3127 (8)	38 (6)	C(48)	5010 (14)	2569 (22)	3726 (9)	45 (6)
C(17)	922 (12)	5110 (18)	3253 (7)	30 (5)	C(49)	4517 (13)	2026 (23)	4048 (8)	42 (6)
C(18)	485 (13)	6097 (20)	3117 (8)	39 (6)	C(50)	3978 (12)	2726 (19)	4338 (8)	35 (5)
C(19)	−336 (16)	6042 (25)	3149 (9)	60 (8)	C(51)	2621 (11)	3879 (17)	4929 (7)	29 (5)
C(20)	−721 (15)	5084 (22)	3312 (9)	50 (7)	C(52)	2554 (11)	3745 (18)	5435 (7)	31 (5)
C(21)	−286 (14)	4083 (22)	3455 (8)	43 (6)	C(53)	1979 (13)	3026 (21)	5616 (8)	44 (6)
C(22)	506 (15)	4123 (24)	3410 (9)	52 (7)	C(54)	1476 (14)	2472 (20)	5297 (8)	41 (6)
C(23)	2292 (12)	3779 (15)	2986 (6)	23 (4)	C(55)	1545 (13)	2619 (19)	4793 (8)	35 (6)
C(24)	2951 (10)	3269 (16)	3160 (7)	24 (5)	C(56)	2121 (12)	3304 (17)	4589 (8)	36 (5)
C(25)	3229 (13)	2191 (20)	2945 (8)	37 (6)					

[a] Equivalent isotropic U defined as one-third of the trace of the orthogonalized U_{ij} tensor.

asymmetric unit. There is no bonding between these entities. The shortest Pb···O contact is 6.44 (2) Å.

Figure 1 shows a view of the entire complex at the top and a view of the inner coordination environment of the lead from a different perspective at the bottom. The lead ion is three-coordinate and pyramidal with a stereochemically active lone pair. The two ligands are not equivalent. One is bound through its two phosphorus atoms as a chelate. The PbP_2C ring is nearly planar with a 178.2° dihedral angle between the PbP_2 and P_2C planes. The other ligand is bound to lead through carbon in a monodentate fashion. Thus it acts as a very bulky alkyl group. The phosphorus atoms in this ligand are uncoordinated. There are significant differences between the P–C distances and the P–C–P angles in the two ligands. The P–C bonds (1.733 (16), 1.747 (16) Å) in the chelating ligand are shorter than the P–C bonds (1.874 (16), 1.830 (16) Å) of the monodentate ligand. This is due to the delocalization of the lone pair over the P–C–P unit and the resulting partial-double-bond character within the chelate. The P–C–P angle (109.3 (7)°) in the chelate ring is less than the corresponding angle (118.2 (7)°) in the monodentate ligand as a result of the constraints of the four-membered ring.

X-ray Crystal Structure of $Pb[(Ph_2P)_2C(SiMe_3)]_2$ (2). Final atomic positional and thermal parameters are set out in Table III. Selected interatomic distances and angles are given in Table IV. Complex **2** crystallizes as a discrete molecule with no unusual contacts between molecules.

Figure 2 shows a view of the entire complex at the top and a diagram of the inner coordination sphere of the lead at the bottom. The lead ion is four-coordinate. Both ligands are nearly equivalent and chelating. Thus comparison with **1** indicates that the bulky trimethylsilyl substituent has inhibited the formation of a Pb–C bond.

The complex has no crystallographically imposed symmetry, but there is an approximate C_2 axis that bisects the P(1)–Pb–P(3) and P(2)–Pb–P(4) angles. The four phosphorus atoms are not equivalent but are grouped into two subunits. Thus P(1) and P(3) are nearly equivalent as are P(2) and P(4). The Pb–P(1) and Pb–P(3) distances (2.715 (5), 2.724 (6) Å) are nearly equal and

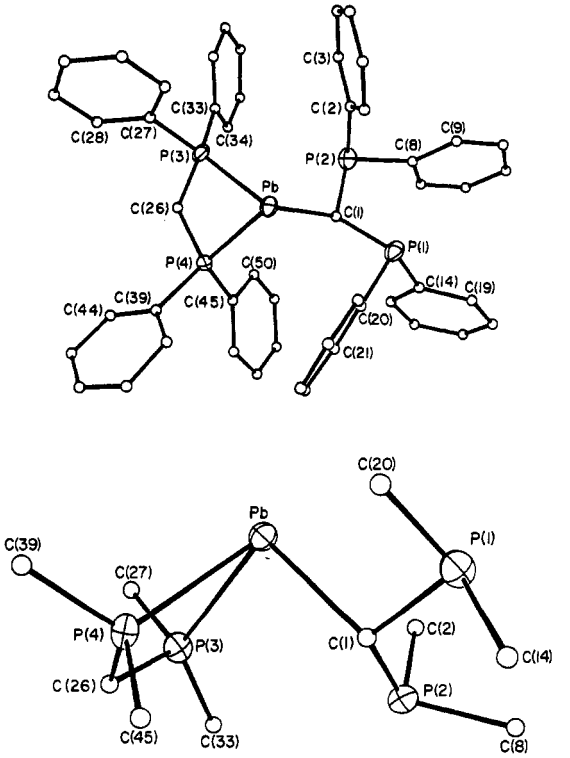

Figure 1. Perspective drawings of $Pb[(Ph_2P)_2CH]_2$ (**1**): top, the entire molecule; bottom, the inner lead coordination with phenyl groups omitted.

are significantly shorter than the Pb–P(2) and Pb–P(4) distances (2.971 (5), 2.889 (6) Å). Likewise the P(1)–Pb–P(3) angle (110.1 (2)°) is significantly compressed relative to the P(2)–Pb–P(4) angle (143.8 (2)°). These irregularities suggest that the lead stereochemistry is not based on square pyramidal geometry but rather that it is best considered as distorted-trigonal-pyramidal

Table IV. Interatomic Distances (Å) and Angles (deg) for $Pb[(Ph_2P)_2C(SiMe_3)]_2$ (**2**)

	Distances		
Pb–P(1)	2.715 (5)	Pb–P(2)	2.971 (5)
Pb–P(3)	2.724 (6)	Pb–P(4)	2.889 (6)
P(1)–C(1)	1.74 (2)	P(1)–C(5)	1.84 (2)
P(1)–C(11)	1.81 (2)	P(2)–C(1)	1.77 (2)
P(2)–C(17)	1.81 (2)	P(2)–C(23)	1.83 (2)
P(3)–C(29)	1.68 (2)	P(3)–C(45)	1.88 (2)
P(3)–C(51)	1.85 (2)	P(4)–C(29)	1.77 (2)
P(4)–C(33)	1.85 (2)	P(4)–C(39)	1.87 (2)
Si(1)–C(1)	1.84 (2)	Si(1)–C(2)	1.89 (2)
Si(1)–C(3)	1.87 (3)	Si(1)–C(4)	1.94 (2)
Si(2)–C(29)	1.86 (2)	Si(2)–C(30)	1.91 (2)
Si(2)–C(31)	1.93 (2)	Si(2)–C(32)	1.92 (3)
	Angles		
P(1)–Pb–P(2)	59.4 (2)	P(1)–Pb–P(3)	110.1 (2)
P(2)–Pb–P(3)	97.6 (2)	P(1)–Pb–P(4)	99.7 (2)
P(2)–Pb–P(4)	143.8 (2)	P(3)–Pb–P(4)	59.8 (2)
Pb–P(1)–C(1)	100.4 (6)	Pb–P(1)–C(5)	130.3 (7)
C(1)–P(1)–C(5)	111.7 (9)	Pb–P(1)–C(11)	97.2 (6)
C(1)–P(1)–C(11)	114.3 (9)	C(5)–P(1)–C(11)	102.4 (10)
Pb–P(2)–C(1)	91.0 (6)	Pb–P(2)–C(17)	102.1 (7)
C(1)–P(2)–C(17)	110.1 (9)	Pb–P(2)–C(23)	137.3 (6)
C(1)–P(2)–C(23)	109.3 (8)	C(17)–P(2)–C(23)	105.2 (9)
Pb–P(3)–C(29)	99.4 (7)	Pb–P(3)–C(45)	130.0 (7)
C(29)–P(3)–C(45)	111.3 (10)	Pb–P(3)–C(51)	97.0 (6)
C(29)–P(3)–C(51)	115.4 (9)	C(45)–P(3)–C(51)	103.6 (9)
Pb–P(4)–C(29)	91.4 (7)	Pb–P(4)–C(33)	103.9 (7)
C(29)–P(4)–C(33)	113.1 (9)	Pb–P(4)–C(39)	136.4 (7)
C(29)–P(4)–C(39)	110.3 (10)	C(33)–P(4)–C(29)	101.5 (10)
C(1)–Si(1)–C(2)	113.1 (10)	C(1)–Si(1)–C(3)	110.1 (10)
C(2)–Si(1)–C(3)	106.8 (11)	C(1)–Si(1)–C(4)	110.1 (10)
C(2)–Si(1)–C(4)	105.7 (11)	C(3)–Si(1)–C(4)	111.0 (12)
C(29)–Si(2)–C(30)	107.5 (9)	C(29)–Si(2)–C(31)	109.5 (9)
C(30)–Si(2)–C(31)	109.9 (10)	C(29)–Si(2)–C(32)	113.7 (10)
C(30)–Si(2)–C(32)	108.6 (11)	C(31)–Si(2)–C(32)	107.6 (11)
P(1)–C(1)–P(2)	107.4 (9)	P(1)–C(1)–Si(1)	124.2 (11)
P(2)–C(1)–Si(1)	127.3 (11)	P(3)–C(29)–P(4)	108.4 (10)
P(3)–C(29)–Si(2)	127.8 (12)	P(4)–C(29)–Si(2)	122.9 (11)

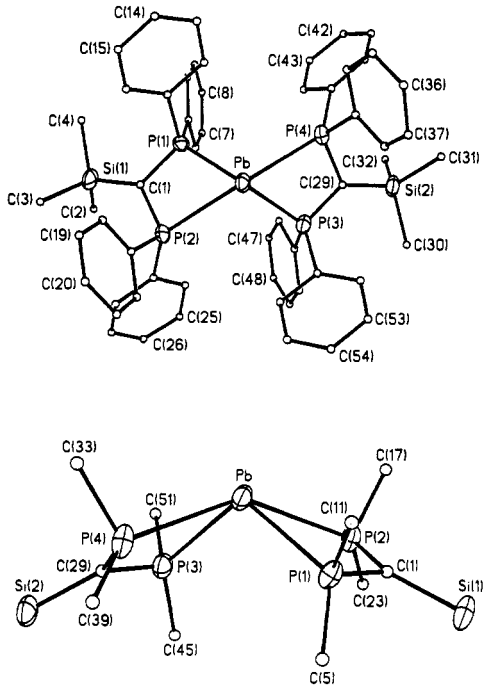

Figure 2. Perspective drawings of $Pb[(Ph_2P)_2C(SiMe_3)]_2$ (**2**): top, the entire molecule; bottom, the inner lead coordination with phenyl groups omitted.

geometry with P(2) and P(4) occupying axial sites while P(1), P(3), and the lead lone pair reside in equatorial sites.

The chelate rings in **2** are nearly planar with only slight folding along the P–P axis. The dihedral angle between the P(1)C(1)P(2) plane and the PbP(1)P(2) plane is 165.9°. The other ring is less folded with a dihedral angle of 169.2° between the P(3)C(29)P(4) plane and the P(3)PbP(4) plane. In both cases the direction of the folding places the carbon atoms C(1) and C(29) closer to the lone pair on lead and moves these atoms, and the appended $SiMe_3$ groups, away from contact with some of the phenyl rings. The geometry at C(1) and C(29) is planar. The sum of the three bond angles about C(1) is 358.9°, while the similar sum for C(29) is 359.1°. This, coupled with the relatively short P–C distances within the chelate rings, indicates that the lone pair created by deprotonation of these carbon atoms is delocalized over the P–C–P unit. The decrease in the P–C–P angles below the ideal of 120° is, of course, a consequence of forming the strained, four-membered chelate rings. There is no apparent reason for the asymmetry at C(29) (i.e. short P(3)–C(29) and long P(4)–C(29) distances and wide P(3)–C(29)–Si(2) and contracted P(4)–C(29)–Si(2) angles), but local packing forces may be involved.

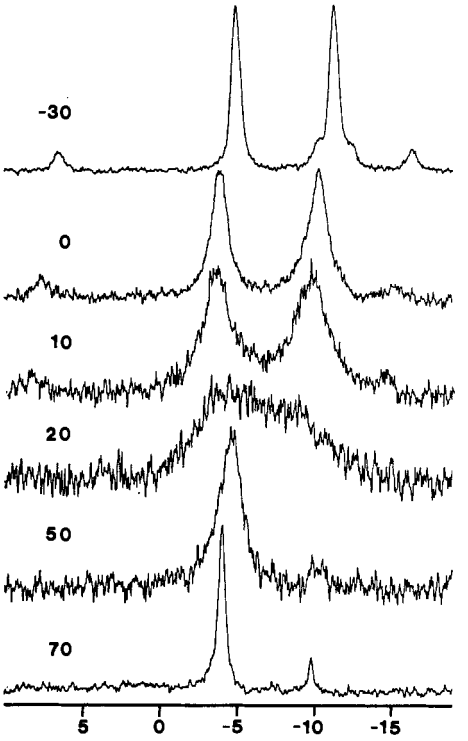

Figure 3. 81-MHz ^{31}P NMR spectra of $Pb[(Ph_2P)_2CH]_2$ (**1**) in toluene solution over the temperature range +70 to −30 °C.

^{31}P NMR Spectral Studies. The ^{31}P NMR spectra of both **1** and **2** show evidence for fluxionality in solution. For **1** two separate processes are observed. The spectra in Figure 3 show the spectral changes occurring over the range +70 to −30 °C. At −30 °C two resonances are seen. The one at −4.7 ppm is assigned, on the basis of the large $^1J(Pb,P)$ (1970 Hz), to the chelating ligand with the direct Pb–P bonds. The other, at −11.6 ppm, which shows satellites with much smaller $^2J(Pb,P)$ (165 Hz), is assigned to the C-bound, monodentate ligand, which lacks direct Pb–P bonding. On warming, these resonances broaden and eventually coalesce into a single, relatively narrow resonance at 70 °C.[20] This process then is one which interchanges the two different types of ligands as shown in eq 1.

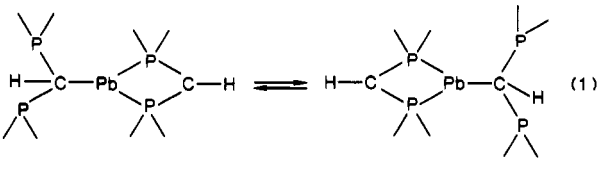

(20) There is a significant temperature dependence of the chemical shifts in this region. Similar effects are well-known in ^{31}P NMR spectroscopy; see: Hunt, C. T.; Balch, A. L. *Inorg. Chem.* **1982**, *21*, 1641. Dickert, F. L.; Hellmann, S. W. *Anal. Chem.* **1980**, *52*, 996.

Table V. Comparison of Structural Parameters for Four-Coordinate Lead (II) Complexes

	$Pb[(Ph_2P)_2C(SiMe_3)]$ (2)	$Pb(S_2COEt)_2$ (3)	$Pb(S_2CNEt_2)_2$ (4)	$Pb[S_2P(OEt)_2]_2$ (5)	PbTPrP
			Distances (Å)		
Pb–L(ax)	2.969 (8)	2.95 (3)	2.940 (10)	3.022 (6)	2.354 (4)[a]
Pb–L(ax)	2.895 (9)	2.84 (3)	2.885 (11)	2.996 (5)	2.367 (4)[a]
Pb–L(eq)	2.715 (8)	2.79 (3)	2.744 (9)	2.754 (6)	2.377 (4)[a]
Pb–L(eq)	2.712 (9)	2.74 (3)	2.786 (9)	2.790 (6)	2.370 (4)[a]
			Angles (deg)		
L(ax)–Pb–L(ax)	143.4 (2)	137.2 (1.0)	133.2 (4)	138.2 (2)	122.0 (1)[a]
L(eq)–Pb–L(eq)	110.0 (3)	98.1 (9)	96.2 (4)	94.1 (2)	119.0 (1)[a]
L–Pb–L(chelate)	59.1 (2)	64.6 (8)	64.1 (3)	71.1 (2)	75.9 (1), 75.2 (1)
L–Pb–L(chelate)	59.6 (3)	61.6 (8)	61.9 (2)	70.6 (2)	76.4 (1), 75.5 (1)
			Reference		
	this work	7	5	4	24

[a] Square-pyramidal geometry, no distinction between axial and equatorial.

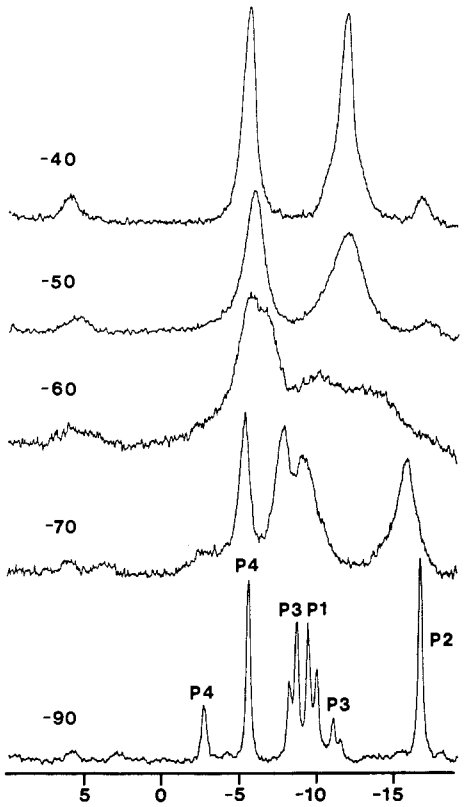

Figure 4. 81-MHz ^{31}P NMR spectra of $Pb[(Ph_2P)_2CH]_2$ (1) in toluene solution over the temperature range −40 to −90 °C. A spectra simulation yields the following parameters from the −90 °C spectrum: $\delta(P(4))$ = −4.5, J(P(4),P(3)) = 240 Hz, $\delta(P(3))$ = −9.9, J(P(3),P(1)) = 47 Hz, $\delta(P(1))$ = −10.1, $\delta(P(2))$ = −17.5.

The low-temperature process is shown in Figure 4. On cooling, the resonances of the two ligand types broaden and then separate into two components. At −90 °C further line narrowing allows spin–spin splitting to be observed. Because of the satellites seen at −30 °C, the resonances labeled P(4) and P(3) arise from the two inequivalent ends of the chelating ligand. The large value of J(P(4),P(3)), 240 Hz, reflects the fact that two pathways for the two-bond, P–P coupling exist and at least one is of considerable magnitude. Resonances P(1) and P(2) arise from the two nonequivalent phosphorus atoms on the monodentate ligand. Coupling between these resonances is too small to be resolved. However, resonances P(3) and P(1) are coupled with ^3J(P(3),P(1)) = 47 Hz. Note that the three-bond phosphorus–phosphorus coupling is smaller than the two-bond phosphorus–phosphorus coupling seen in the chelate ring. The pattern observed at −90 °C, with four distinct phosphorus environments, is entirely in accord with the crystallographic results, which show four unique phosphorus atoms. The absence of any detectable P–P coupling to resonance P(2) while significant coupling between P(3) and P(1) occurs is readily

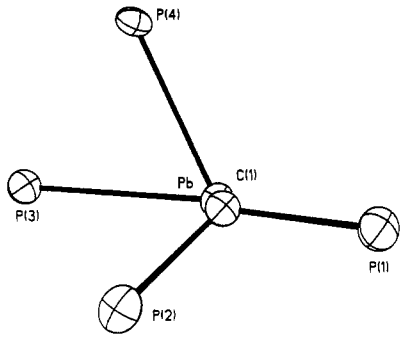

Figure 5. Projection of the structure of $Pb[(Ph_2P)_2CH]_2$ (1) down the Pb–C(1) bond. Only the disposition of the four phosphorus atoms about the bond is indicated.

explained by considering the angular distribution of substituents about the Pb–C(1) bond. A view down that bond is shown in Figure 5. As is readily seen, the P(3)PbC(1)P(1) unit is nearly planar; consequently, from the Karplus relationships, the vicinal P(3)–P(1) coupling should be the largest of the three bond P–P coupling constants while the corresponding P(1)–P(4) coupling should be smaller, and in fact none is detected. For P(2), the angular arrangement indicates that vicinal coupling to P(3) and P(4) should also be smaller than the P(1)–P(3) coupling. Again neither coupling is large enough to be detected. This situation pertains as long as there is restricted rotation about the C(1)–Pb bond. Once free rotation sets in, the two phosphorus atoms P(1) and P(2) can become equivalent and the dissymmetry due to restricted rotation is lost. P(3) and P(4) become equivalent as well once free rotation occurs.[21,22]

In toluene solution at 25 °C the ^{31}P NMR spectrum of 2 consists of a single resonance at 21.8 ppm with satellites due to ^{207}Pb with ^1J(Pb,P) = 1510 Hz. Thus at this temperature the four phosphorus atoms have become equivalent, probably through a process similar to pseudorotation. On cooling, the resonance broadens. At −80 °C at 81 MHz, it has broadened to the point it is lost in the base line. Instrumental limitations prohibited us from observing further changes.

Discussion

Compounds 1 and 2 show two modes of coordination for the diphosphinomethanide ligand. The chelating form has been observed in the planar complex $Pt[(Ph_2P)_2CH]_2$[19] and in the tin(II)

(21) Related observations on 1 have been made by Karsch and co-workers (Karsch, H. H.; Appelt, A.; Hanika, G. *J. Organomet. Chem.* **1986**, *312*, C1). However they do not report observation of the Pb–P satellites, and they interpret the low-temperature process as resulting from restricted rotation about the P–C bonds. While restricted rotation about the P–C bonds may contribute to the barrier to the low-temperature process, we believe that the essential rotation that must occur before equivalence is achieved is rotation about the Pb–C bond. The importance of rotation about this bond is readily apparent from Figure 6.

(22) Brown, M. P.; Yavari, A.; Manojlovic-Muir, L.; Muir, K. W.; Moulding, R. P.; Seddon, K. P. *J. Organomet. Chem.* **1982**, *236*, C33.

analogue of **1**.[16,17,23] The monodentate form has been observed only in **1** and in $Sn[(Ph_2P)_2CH]_2$.[16,17]

Low-coordinate lead(II) complexes such as **1** and **2** are rare. The three-coordinate, pyramidal geometry of **1** is similar to that found for $[Pb(SC_6H_5)_3]^-$ and $[Pb(SeC_6H_5)_3]^-$.[6] Compound **1** is unique in that no other compounds with Pb(II)–C bonds have been structurally characterized by X-ray crystallography, and only one other example with Pb(II)–P bonding has been so characterized.[13]

Four-coordinate lead(II) complexes are somewhat more common. The bis(bidentate) complexes, $Pb(S_2COEt)_2$ (**3**),[7] $Pb(S_2CNEt_2)_2$ (**4**),[5] and $Pb[S_2P(OEt)_2]_2$ (**5**)[4] are particularly relevant because of their structural similarities. These, along with **2**, possess a distorted-trigonal-bipyramidal geometry with a lead lone pair that occupies an equatorial site and with severe constraints due to the four-membered chelate rings. Comparison of structural data for the lead coordination of these compounds is given in Table V. All have two sets of Pb–ligand distances: long ones to the axial sites and shorter ones to the equatorial sites. The L(ax)–Pb–L(ax) angles in all cases are considerably less than the ideal 180°. The L(eq)–Pb–L(eq) angles are also less than the ideal 120°. These angular distortions are clearly attributable to the effects of the four-membered chelate rings, which produce considerable constraints on the angular ligand distribution. In contrast, the other lead(II) four-coordinate complex, (*meso*-tetra-*n*-propylporphyrinato)lead(II) (PbTPrP), has square-pyramidal geometry with the lead bound to four equivalent nitrogens and sitting 1.174 Å out of the N_4 plane.[24] Comparison of the structural data in Table V demonstrates the greater symmetry of the porphyrin complex.

The structure of **2** is also related to that of the tin(II) complex $Sn[(Me_2P)_3C]_2$ (**7**).[23] As with **2**, the ligand binds in a chelate

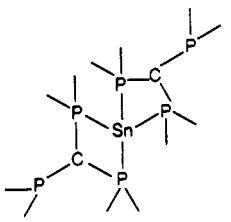

7

fashion with one PMe_2 group on each ligand uncoordinated. This complex also adopts a trigonal-bipyramidal geometry like that of **2**. A major structural difference between **2** and **7** involves the slight folding of the chelate rings. The folding in **2** is less than that in **7**. The dihedral angles between the PbP_2 and P_2C planes in **2** are 165.9 and 169.2° while the corresponding angles between SnP_2 and P_2C planes in **7** are 159.7 and 164.6°. However, the direction of this folding is reversed in the two molecules. Thus in **2**, C(1) and C(29) are displaced 0.253 and 0.189 Å out of the PbP_2 plane in the direction toward the lead lone pair. Presumably this relieves steric crowding between the $SiMe_3$ group and the phenyl groups. In **7**, however, the corresponding carbons are displaced 0.41 and 0.27 Å out of the SnP_2 plane in the direction away from the lone pair.[23] The interpretation[23] that this folding results from lone-pair repulsion is now open to question.

Experimental Section

Preparation of Compounds. Bis(diphenylphosphino)(trimethylsilyl)-methane[19] was prepared as described previously. Bis(diphenylphosphino)methane (Aldrich) was recrystallized from diethyl ether in order to remove the chloroform that Aldrich used to purify this material. Lead(II) chloride (Alfa) was dried under vacuum 30 min before use. Solvents were carefully dried and purged of oxygen before use. All reagents and products were handled with the exclusion of air by standard Schlenk techniques.

$Pb[(Ph_2P)_2CH]_2$ (1). A solution of 2.93 mL of 1.6 M *n*-butyllithium (4.69 mmol) was added via syringe with stirring to a solution of bis(diphenylphosphino)methane (1.50 g, 3.90 mmol) in 30 mL of THF at 0 °C. The solution was allowed to come to room temperature before use. It was added dropwise to an ice-cold, stirred mixture of lead(II) chloride (0.543 g, 1.95 mmol) in 30 mL of THF. After the addition was completed, the reaction mixture was allowed to come to room temperature. This resulted in an opaque gray/black colored mixture with a fine dispersion of lead metal. The THF was removed under vacuum, and the product was redissolved in 40 mL of diethyl ether. Filtration of this mixture through a bed of Celite yielded a clear, deeply orange solution. Concentration of this solution to about 25 mL and slow cooling to −10 °C gave 1.05 g of orange needles in 55% yield.

$Pb[(Ph_2P)_2C(SiMe_3)]_2$ (2). A solution of 2.0 mL of *n*-butyllithium (3.2 mmol) was added to a stirred solution of 1.24 g (2.72 mmol) of bis(diphenylphosphino)(trimethylsilyl)methane in 30 mL of THF at 0 °C. This solution was warmed to room temperature and then added dropwise to a solution of 0.38 g (1.35 mmol) of lead(II) chloride in 30 mL of THF at 0 °C. After being stirred for 1 hour, the deep orange solution was evaporated to dryness and the residue was redissolved in ethyl ether. After filtration through Celite and evaporation to about 25 mL, the solution was cooled to −10 °C. Deep orange crystals formed; yield 1.25 g (82%).

Spectroscopic Measurements. The ^{31}P spectra were recorded with proton decoupling on a Nicolet NT-200 Fourier transform spectrometer operating at 81 MHz or on a Nicolet NT-360 spectrometer at 145.8 MHz. The reference was external 85% phosphoric acid. The high-frequency positive convention, recommended by IUPAC, was used in reporting all chemical shifts.

X-ray Data Collection. $Pb[(Ph_2P)_2CH]_2 \cdot (C_2H_5)_2O$ (1). Brown crystals of **1** were formed by slowly cooling an ether solution of the compound. The crystals were removed from the Schlenk tube under a stream of dry nitrogen and quickly covered with a light hydrocarbon oil to protect them from the atmosphere. Unit cell parameters were obtained from a least-square refinement of 21 reflections with $15 < 2\theta < 20°$. The space group $P2_1/c$ (No. 14) was uniquely determined by the following observed conditions: $h0l$, $l = 2n$, and $0k0$, $k = 2n$. No decay in the intensities of two standard reflections occurred. Data collection parameters are summarized in Table VI. The data were corrected for Lorentz and polarization effects.

$Pb[(Ph_2P)_2C(SiMe_3)]_2$ (2). Bright orange bicapped parallelepipeds of **2** were formed by slowly cooling a saturated solution of the compound. In a drybox, the crystals were removed from the Schlenk tube and covered with a light hydrocarbon oil to protect them from the atmosphere. The lattice was found to be orthorhombic *P* by standard procedures using the software of the Syntex $P2_1$ diffractometer. The data were collected at 130 K by using a locally modified LT-1 apparatus on the diffractom-

Table VI. Crystal Data for $Pb[(Ph_2P)_2CH]_2$ and $Pb[(Ph_2P)_2C(SiMe_3)]_2$

	1	2
formula	$C_{54}H_{52}OP_4Pb$	$C_{56}H_{58}P_4PbSi_2$
fw	1048.05	1118.23
cryst syst	monoclinic	orthorhombic
space group	$P2_1/c$	$P2_12_12_1$
cryst dimens, mm	0.63 × 0.10 × 0.15	0.13 × 0.18 × 0.37
color and habit	orange parallelepipeds	orange bicapped parallelpipeds
unit cell dimens (130 K)		
a, Å	18.075 (8)	17.252 (43)
b, Å	14.713 (6)	11.331 (12)
c, Å	18.099 (8)	26.600 (40)
β, deg	92.29 (4)	
V, Å^3	4810 (4)	5200 (16)
D_{calcd}, g/cm^3 (130 K)	1.38	1.43
Z	4	4
radiatn; λ, Å (graphite monochromator)	Mo Kα; 0.71069	Mo Kα; 0.71069
μ(Mo Kα), cm^{-1}	36.21	33.96
transmissn factors	0.549–0.527	0.483–0.373
scan type	ω	ω
$2\theta_{max}$, deg	50	50
scan range, deg	1.8	2.2
octants	$+h,+k,\pm l$	$+h,+k,+l$
scan speed, deg/min	20	5
check reflcns; interval no.	2; 198	3; 197
no. of unique data	8480	5114
no. of data $I > 3\sigma(I)$	3899	2854
R	0.057	0.053
R_w	0.052	0.055
no. of params	272	288

(23) Karsch, H. H.; Appelt, A.; Müller, G. *Organometallics*. **1986**, *5*, 1664.
(24) Barkigia, K. M.; Fajar, J.; Adler, A. D.; Williams, G. J. B. *Inorg. Chem.* **1980**, *19*, 2057.

eter. Printer plots of several reflections using ω scans revealed a small peak on the left side of the main peaks. This was true of several crystals mounted. It was found that the whole peak could be collected by using a relatively large scan range of 2.2°. With this scan range, the data were collected in a standard manner. The space group $P2_12_12_1$ (No. 19) was uniquely determined by the following observed conditions: $h00$, $h = 2n$, $0k0$, $k = 2n$, and $00l$, $l = 2n$. No decay in the intensities of three standard reflections occurred. Data collection parameters are summarized in Table VI. The data were corrected for Lorentz and polarization effects.

Solution and Refinement of Structure. $Pb[(Ph_2P)_2CH]_2\cdot(C_2H_5)_2O$ (1). All structure determination calculations were done on a Data General Eclipse MV/10000 computer using the SHELXTL version 4 software package. The position of the lead and two of the phosphorus atoms were generated by direct methods. Other atom positions were located from successive difference Fourier maps. Anisotropic thermal parameters were assigned to the lead and phosphorus atoms, and isotropic thermal parameters were used for the remaining atoms. The final R value of 0.057 was computed from 272 least-square parameters and 1902 reflections. This yielded a goodness-of-fit of 1.22 and a mean shift/esd of 0.053 for rotation of the methyl group at C(54) on the last cycle of refinement. A value of 0.58 e/Å^3 (less than that expected for a hydrogen atom) was found as the largest feature on the final difference Fourier map. This peak was 1.24 Å from the tin atom. The weighting scheme used was $w = [\sigma^2(F_o)]^{-1}$. Correction for absorption were applied.[25] Neutral-atom scattering factors were those of Cromer and Waber.[26]

$Pb[(Ph_2P)_2C(SiMe_3)]_2$ (2). The position of the lead atom was found from the Patterson map. Other atom positions were located from successive difference Fourier maps. Anisotropic thermal parameters were assigned to lead, phosphorus, and silicon while isotropic thermal parameters were used for the remaining atoms. Refinement of these atoms converged at $R = 0.105$. The final stages of refinement included an absorption correction (XABS).[22] The handedness of the crystal was determined by use of a SHELXTL routine. This required inversion of the structure from the coordinates originally chosen. The correct hand converges with an R value of 0.053 while the incorrect one converges at an R value of 0.079. All hydrogen atoms were fixed at calculated positions by using a riding model in which the C–H vector was fixed at 0.98 Å, and the thermal parameter for each hydrogen atom was set at 1.2 times the value for the carbon atom to which it was bonded. A goodness-of-fit of 0.910 and a mean shift/esd of 0.006 for overall scale was calculated on the last cycle of refinement. A value of 0.97 e/Å^3 was found as the largest feature on the final difference Fourier map. This was 0.97 Å away from the lead atom and is probably a consequence of the relatively wide peaks of this crystal.

Acknowledgment. We thank the National Science Foundation (Grant CHE 8519557) for financial support. D.E.O. was a Earl C. Anthony Fellow.

Supplementary Material Available: A stereoview of **2** and listings of all bond lengths, bond angles, anisotropic thermal parameters, and hydrogen atom positional and thermal parameters for **1** and **2** (9 pages); listings of structure factor amplitudes for **1** and **2** (41 pages). Ordering information is given on any current masthead page.

(25) Hope, H.; Mozzi, B. "XABS, an absorption correction program producing an absorption tensor from an expression relating F_o and F_c"; Department of Chemistry, University of California, Davis, CA, unpublished results.

(26) *International Tables for X-ray Crystallography*; Kynoch: Birmingham, England, 1974; Vol. IV: (a) pp 149–150; (b) pp 99–101.

Contribution from the Chemistry and Materials Science Divisions, Argonne National Laboratory, Argonne, Illinois 60439, and Department of Chemistry, North Carolina State University, Raleigh, North Carolina 27650

Synthesis and Structure of ζ-$(BEDT\text{-}TTF)_2(I_3)(I_5)$ and $(BEDT\text{-}TTF)_2(I_3)(TlI_4)$: Comparison of the Electrical Properties of Organic Conductors Derived from Chemical Oxidation vs. Electrocrystallization

Mark A. Beno,*† Urs Geiser,† Kim L. Kostka,† Hau H. Wang,† Kevin S. Webb,† Millicent A. Firestone,† K. Douglas Carlson,† Luis Nuñez,† Myung-Hwan Whangbo,‡ and Jack M. Williams†

Received December 30, 1986

Chemical oxidation of bis(ethylenedithio)tetrathiafulvalene (BEDT-TTF or ET, $C_{10}S_8H_8$) in benzonitrile solution by slow diffusion of iodine vapor produces a mixture of black lustrous crystals. These include the well-known α- and β-$(ET)_2I_3$ phases, δ-$(ET)I_3$, and ϵ-$(ET)_2(I_3)(I_8)_{0.5}$, as well as a new phase, ζ-$(ET)_2(I_3)(I_5)$. Single-crystal X-ray diffraction studies show that this latter salt is monoclinic, $P2_1/a$, with $a = 15.113$ (4) Å, $b = 15.993$ (6) Å, $c = 18.159$ (9) Å, $\beta = 100.99$ (3)°, $V_c = 4308$ (2) Å^3, and $Z = 4$. The crystal structure consists of two-dimensional sheets containing both ET donor molecules and I_3^- anions, and these mixed ET–I_3^- sheets are separated by layers of V-shaped I_5^- anions. This ζ-phase is structurally very similar to ϵ-$(ET)_2(I_3)(I_8)_{0.5}$. Four-probe resistivity measurements of single crystals of ϵ-$(ET)_2(I_3)(I_8)_{0.5}$ and ζ-$(ET)_2(I_3)(I_5)$ both prepared by the present chemical oxidation method show that, although these materials are metallic to temperatures as low as 1.7 K, they do not undergo transitions to the superconducting state. These findings were confirmed by radio-frequency (rf) field penetration depth measurements of the same samples, which failed to detect superconductivity down to temperatures of 0.5 K. Band electronic structure calculations based on the crystal structure parameters of ϵ-$(ET)_2(I_3)(I_8)_{0.5}$ and ζ-$(ET)_2(I_3)(I_5)$ predict semiconducting properties for stoichiometric crystals. Therefore, it is proposed that the observed metallic properties result from the presence of anion vacancies producing slightly nonstoichiometric crystals. A new salt $(ET)_2(I_3)(TlI_4)$ was prepared by electrochemical oxidation, and a crystal structure study reveals that it is monoclinic, $P2_1/n$, with $a = 8.348$ (3) Å, $b = 15.294$ (8) Å, $c = 34.217$ (16) Å, $\beta = 93.61(3)$°, $V_c = 4360$ (3) Å^3, and $Z = 4$. As in the case of ϵ-$(ET)_2(I_3)(I_8)_{0.5}$ and δ-$(ET)_2(I_3)(I_5)$, $(ET)_2(I_3)(TlI_4)$ consists of mixed two-dimensional sheets containing both ET donor molecules and I_3^- anions, which are separated by layers of tetrahedral TlI_4^- ions. The salt is a semiconductor, in agreement with our band structure calculations.

Introduction

Electrolytic oxidation of bis(ethylenedithio)tetrathiafulvalene[1] (BEDT-TTF or ET, $C_{10}S_8H_8$) in the presence of triiodide anions leads to the ambient-pressure organic superconductors β-$(ET)_2I_3$ (superconducting transition temperature $T_c = 1.5$ K)[2,3] and γ-$(ET)_3(I_3)_{2.5}$ ($T_c = 2.5$ K),[4,5] as well as nonsuperconducting α-$(ET)_2I_3$[6] and δ-$(ET)I_3$.[5] Of these salts, the δ- and γ-phases are reportedly synthesized by electrocrystallization in 1,1,2-tri-

(1) Williams, J. M.; Beno, M. A.; Wang, H. H.; Leung, P. C. W.; Emge, T. J.; Geiser, U.; Carlson, K. D. *Acc. Chem. Res.* **1985**, *18*, 261.
(2) Yagubskii, E. B.; Shchegolev, I. F.; Laukhin, V. N.; Kononovich, P. A.; Kartsovnik, M. V.; Zvarykina, A. V.; Buravov, L. I. *JETP Lett.* (*Engl. Transl.*) **1984**, *39*, 12.
(3) Williams, J. M.; Emge, T. J.; Wang, H. H.; Beno, M. A.; Copps, P. T.; Hall, L. N.; Carlson, K. D.; Crabtree, G. W. *Inorg. Chem.* **1984**, *23*, 2558.

† Argonne National Laboratory.
‡ North Carolina State University.

0020-1669/87/1326-1912$01.50/0